

Research Article

Application of Surface Spline Interpolation Method in Parameter Estimation of a PM_{2.5} Transport Adjoint Model

Ning Li,^{1,2} Xianqing Lv ,² and Jicai Zhang ³

¹School of Science, Dalian Jiaotong University, Dalian 116028, China

²Physical Oceanography Laboratory/CIMST, Ocean University of China and Qingdao National Laboratory for Marine Science and Technology, Qingdao 266003, China

³Institute of Physical Oceanography, Ocean College, Zhejiang University, Zhoushan 316000, China

Correspondence should be addressed to Jicai Zhang; jicai_zhang@163.com

Received 31 March 2018; Accepted 21 June 2018; Published 5 July 2018

Academic Editor: Shuo Wang

Copyright © 2018 Ning Li et al. This is an open access article distributed under the Creative Commons Attribution License, which permits unrestricted use, distribution, and reproduction in any medium, provided the original work is properly cited.

A new method for the estimation of initial conditions (ICs) in a PM_{2.5} transport adjoint model is proposed in this paper. In this method, we construct the field of ICs by interpolating values at independent points using the surface spline interpolation. Compared to the traditionally used linear interpolation, the surface spline interpolation has an advantage for reconstructing continuous smooth surfaces. The method is verified in twin experiments, and the results indicate that this method can produce better inverted ICs and less simulation errors. In practical experiments, simulation results show good agreement with the ground-level observations during the 22nd Asia-Pacific Economic Cooperation summit period, demonstrating that the new method is effective in practical application fields.

1. Introduction

In recent years, air pollution has escalated to hazardous levels in Chinese cities. Among numerous types of air pollution, PM_{2.5} (fine particles with diameter of 2.5 μm or less) is considered the most threatened kind to life expectancy and public health (e.g., [1–4]). Therefore, simulation and prediction of PM_{2.5} pollution are always an area of interest to researchers.

An increasing number of atmospheric numerical models have been conducted and publicly available in various studies for more in-depth understanding of the physical, chemical, and dynamical processes concerned with PM_{2.5} pollution (e.g., [5–12]). Initial condition (IC) plays an important role in the model researches. Providing the best possible ICs is essential for the success of the models. Existing studies presented several methods to obtain the IC. The initial condition was obtained from the National Meteorological Center (NMC) global data and enhanced by rawinsonde and surface observations by Liu et al. [11]. A background value (a small constant) was given to the model with the first few

days as the spin-up period to minimize the influence of initial conditions by Fu et al. [12]. Another efficient and accurate way to estimate the ICs is through data assimilation using the adjoint method (e.g., [13–17]).

Data assimilation provides a configuration for combining observations and models to form an optimal initial model state. In this method, uncertain model parameters can be constrained by minimizing the distance between the model simulations and observations. In practice, how to reduce the influence of ill-posedness caused by excessive control parameters has been a key part of data assimilation and parameter estimation. Several studies have proved that it can be effectively solved by applying independent point scheme (IPS) (e.g., [13–17]). In detail, several grids are selected as independent points (IPs) in the space domain; values of the ICs at the IPs can be optimized, while those at other grids can be calculated through a certain interpolation method with the values at the IPs. Thus interpolation is another important problem that remains to be studied.

Referring to previous studies, Cressman interpolation (hereafter abbreviated as CI) is preferred for the adjoint

model due to easy accessibility. Although the adjoint model with the CI leads to satisfying results in general, the reconstructed IC field is unsmooth around the independent points [18]. Therefore, a more reasonable interpolation method needs to be found to combine with the adjoint method.

The surface spline interpolation, with a special type of piecewise polynomial called spline, is widely used as one popular technique for data interpolation. The surface spline is a powerful tool for interpolating irregular, continuous geological or other surfaces, and is often better than polynomial interpolation because the interpolation error can be made very small [19]. Many real applications of the surface spline method indicate that the results are usually appropriate for oceanographic and meteorological contexts and it is particularly good for inferring smooth structure from scattered data. As stated in the work of Harder et al. [20], the surface spline was proposed to interpolate wing deflections and computing slopes for aeroelastic calculations. Based on the surface spline interpolation, a new mathematical model for tropical cyclone wind speeds is proposed in [21]. Compared with the earlier wind model with linear interpolation, the surface spline model could produce a more accurate wind estimate. In [22], Yaghoobi et al. described a scheme based on a cubic spline interpolation which is applied to approximating the variable-order fractional integrals and is extended to solving a class of nonlinear variable-order fractional equations with time delay. Guo and Pan [18] validated this new IP scheme with twin experiments, and the results showed that the prescribed nonlinear distribution of bottom friction coefficients are better inverted with the surface spline interpolation. Due to its proved superior performance, the surface spline interpolation (SSI) is applied to inversion of ICs with a PM_{2.5} transport adjoint model in this study.

The paper is organized as follows. Section 2 provides the detailed descriptions of the numerical model and implementation of SSI. Twin experiments and practical experiments are carried out to evaluate the performance of SSI in inversion of ICs in Sections 3 and 4, respectively. Finally, some key conclusions drawn from the work are presented in Section 5.

2. Numerical Model and Settings

2.1. Forward Model. The governing equations of the two-dimensional PM_{2.5} transport model are as follows:

$$\frac{\partial C}{\partial t} + u \frac{\partial C}{\partial x} + v \frac{\partial C}{\partial y} = \frac{\partial}{\partial x} \left(A_H \frac{\partial C}{\partial x} \right) + \frac{\partial}{\partial y} \left(A_H \frac{\partial C}{\partial y} \right) + S \quad (1)$$

$$C(t^0, x, y) = C^0(x, y) \quad (2)$$

where C denotes the ground-level PM_{2.5} concentration, u and v are the horizontal wind velocity in x -coordinate and y -coordinate, respectively, A_H is the horizontal diffusivity coefficient, S is the value of the source and sink, and C^0 is the initial condition (IC) to be estimated in this study.

The boundary conditions are set as constant at the inflow boundary Γ^{IN} and no gradient boundary conditions at the outflow boundary Γ^{OUT} .

$$\frac{\partial C}{\partial t} = 0 \quad \text{on } \Gamma^{\text{IN}} \quad (3)$$

$$\frac{\partial C}{\partial \vec{n}} = 0 \quad \text{on } \Gamma^{\text{OUT}} \quad (4)$$

2.2. Adjoint Model. The adjoint model is defined to calculate the gradients of the cost function with respect to various input parameters, which incorporate all physical processes included in the governing model, to obtain the minimization of the distance between the model output and observations. Based on the governing equations (1)–(4), its adjoint model can be constructed as follows.

First, the distance is expressed by the cost function which is defined as

$$J = \frac{1}{2} \int_{\Sigma} K (C - C_{\text{obs}})^2 d\sigma \quad (5)$$

where Σ denotes the set of the observations in time and space domain and C and C_{obs} are the simulated and observed PM_{2.5} concentrations, respectively. And K is the weighting matrix and should be the inverse of observation error covariance matrix theoretically. K can be fixed simply, assuming that the errors in the data are uncorrelated and equally weighted. In the present model, K is 1 when the observations are available and 0 otherwise.

Then the Lagrangian function is constructed based on the theory of Lagrangian multiplier method and can be expressed as

$$L = J + \int \left\{ p \times \left[\frac{\partial C}{\partial t} + u \frac{\partial C}{\partial x} + v \frac{\partial C}{\partial y} - \frac{\partial}{\partial x} \left(A_H \frac{\partial C}{\partial x} \right) - \frac{\partial}{\partial y} \left(A_H \frac{\partial C}{\partial y} \right) - S \right] \right\} d\sigma \quad (6)$$

where p is the adjoint variable of C .

According to the typical theory of Lagrangian multiplier method, we have the following first-order derivatives of Lagrangian function with respect to all the variables and parameters:

$$\frac{\partial L}{\partial p} = 0 \quad (7)$$

$$\frac{\partial L}{\partial A_H} = 0, \quad (8)$$

$$\frac{\partial L}{\partial S} = 0$$

$$\frac{\partial L}{\partial C} = 0 \quad (9)$$

Equation (7) gives the governing equation (1) of the forward model. The adjoint equation can be developed from equation (9), which is given as follows:

$$\frac{\partial p}{\partial t} + u \frac{\partial p}{\partial x} + v \frac{\partial p}{\partial y} + \frac{\partial}{\partial x} \left(A_H \frac{\partial p}{\partial x} \right) + \frac{\partial}{\partial y} \left(A_H \frac{\partial p}{\partial y} \right) - K(C - C_{\text{obs}}) = 0 \quad (10)$$

Equations of the adjoint model and the numerical scheme of forward and adjoint equations are similar to Wang et al. [13].

2.3. Optimization of Independent ICs. In this adjoint model, the optimal parameters should be explored to minimize the cost function J . Minimization of the cost function is implemented through parameter optimization. This optimization routine is performed through iterative integrations of the governing and adjoint equations.

According to the steepest decent (SD) method, optimization of the control variable is conducted as follows:

$$k_l^{i+1} = k_l^i - \alpha^i \cdot p_l^i \quad (11)$$

In the above-mentioned equations, i denotes the iteration step, k_l is the l -th parameter, α is the step factor, and N is the number of independent parameters. It should be noted that p is the normalized gradient of J in respect to C^0_l ,

$$p_l = \frac{\partial J / \partial C^0_l}{\sqrt{\sum_{l=1}^N (\partial J / \partial C^0_l)^2}} \quad (12)$$

The optimized gradients of the IC can be obtained by solving the equation $\partial L / \partial C^0 = 0$. We arrive at

$$\frac{\partial J}{\partial C^0} = \left(\frac{\partial p}{\partial t} \right)^0 + (\nabla \cdot \vec{V} p)^0 + (A_H \nabla^2 p)^0 \quad (13)$$

If the ICs at some grid points are selected as independent ICs, we can interpolate these independent ICs to obtain the whole IC by the following equation:

$$k_{i,j} = \sum_{l=1}^N W_{i,j}^l k_l \quad (14)$$

where $k_{i,j}$ is the parameter at the grid point (i,j) , k_l is the l -th independent parameter, and $W_{i,j}^l$ is the coefficient of interpolation. Then the optimized gradients of IC with respect to the l -th independent IC are

$$\frac{\partial \hat{J}}{\partial C^0_l} = \frac{\partial J}{\partial C^0_l} + \sum_{i,j} W_{i,j}^l \frac{\partial J}{\partial C^0_{i,j}} \quad (15)$$

where (i,j) denotes grid points within the influence radius of the l -th independent IC.

Referring to previous studies, the parameters can be obtained by Cressman interpolation (hereafter abbreviated as CI), and the coefficient is traditionally calculated by Zhang et al. [24]:

$$W_{i,j}^l = \frac{w_{i,j}^l}{\sum_{l=1}^N w_{i,j}^l} \quad (16)$$

where $w_{i,j}^l = (R^2 - (r_{i,j}^l)^2) / (R^2 + (r_{i,j}^l)^2)$ is the Cressman weight, $r_{i,j}^l$ is the distance between the grid point (i,j) and the l -th

independent point, and R is the influence radius set based on experience.

In this study, the surface spline interpolation is adopted, and the SSI coefficients are shown as follows.

Assuming that ICs are known at N points, the whole IC filed can be constructed with a variation of the surface spline. The IC at grid points (i,j) is expressed as [25]

$$C^0_{i,j} = \sum_{l=1}^N A_l \left(\frac{r_{ij,l}^2}{R^2} \ln \frac{r_{ij,l}^2}{R^2} + 1 - \frac{r_{ij,l}^2}{R^2} \right) \quad (17)$$

where $r_{ij,k}$ is the distance between the k -th independent point and grid (i,j) , R is a prescribed radius, and A_k is the coefficient to be determined. Actually, the relationship between the known IC and the others can be expressed in matrix form as

$$WX = Y \quad (18)$$

The detailed forms of the three matrixes are given as

$$\begin{aligned} X &= (A_l)_{N \times 1} \\ Y &= (C^0_l)_{N \times 1} \\ W &= (w_{ij})_{N \times N} \end{aligned} \quad (19)$$

where $w_{ij} = \begin{cases} 1, & i=j \\ (r_{ij}^2/R^2) \ln(r_{ij}^2/R^2) + 1 - r_{ij}^2/R^2, & i \neq j \end{cases}$ and r_{ij} is the distance between the i -th and j -th independent points. After calculation, we get

$$A_k = \sum_{l=1}^N M_{kl} C^0_l \quad (20)$$

where $W^{-1} = (M_{kl})_{N \times N}$. By Plugging (17) into (20), we arrive at

$$C^0_{i,j} = \sum_{l=1}^N W_{i,j}^l C^0_l \quad (21)$$

where $W_{i,j}^l = \sum_{k=1}^N M_{kl} ((r_{ij,k}^2/R^2) \ln(r_{ij,k}^2/R^2) + 1 - r_{ij,k}^2/R^2)$ is the coefficient corresponding to the l -th independent IC at the grid (i,j) .

2.4. Independent Point Scheme. Uniform selection of the independent point over the survey region is quite commonly used in the adjoint model (e.g., [14–17]). Although this selecting strategy can be realized easily, but it is not a good choice due to little consideration about the physical characteristics of the research object [18]. As we know, the spatial distribution of $PM_{2.5}$ presents geographic features. If the independent ICs are selected according to the spatial distribution of $PM_{2.5}$, the selection will be more reasonable. At the area where $PM_{2.5}$ concentration is high, more independent points will be needed. Moreover, fewer independent points will be enough at the area with low $PM_{2.5}$ concentration.

High concentration of $PM_{2.5}$ was found in three areas of China: (1) the North China Plain including two of

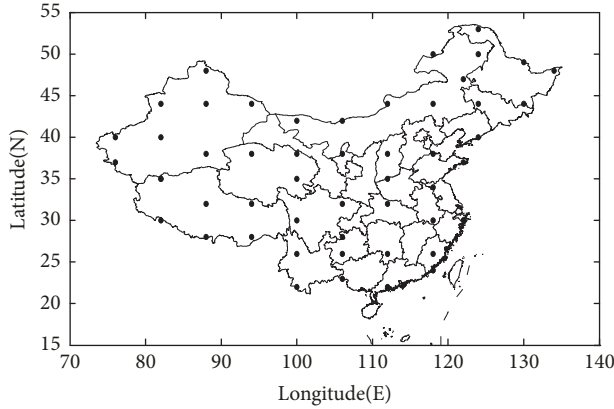


FIGURE 1: Map of computing area and distribution of independent points (dots).

China's four municipalities, Beijing and Tianjin, southern Hebei Province, western Shandong Province, and northern Henan province; (2) the Northeast China Plain; and (3) the Taklimakan desert (e.g., [3, 4]). Therefore, grid points in the above-mentioned high concentration area are selected as independent points from each $5^\circ \times 5^\circ$ area. Grid points in other areas are selected as independent points from each $6^\circ \times 6^\circ$ area. In this study, 67 independent points are selected and shown in Figure 1.

2.5. Settings. The area of modeling computation is China, covering 70° - 140° E and 15° - 55° N, with a space resolution of $0.5^\circ \times 0.5^\circ$. There are 141×71 grids totally in the area. The simulation period is 168 hours and the inverse integral time step is 10 minutes. The wind datasets used in our experiments are the NCEP Final Analysis (GFS-FNL) with spatial resolution of 2.5 degrees and temporal resolution every 24 hours. We get the 0.5-degree data by using bilinear interpolation for space and linear interpolation for time and keep mass conservation of air. The background value is fixed as $15.0 \mu\text{g}/\text{m}^3$. Inflow boundary values are fixed equal to the background values. The horizontal diffusion coefficient A_H is fixed as $100.0 \text{ m}^2/\text{s}$.

Seventy-four major Chinese cities are treated as the observation positions. Labeled as "assimilated cities", the observations at these cities are assimilated in the optimization procedure. Meanwhile, Jinan (JNa), Zhengzhou (ZhZ), Shenyang (SY), Quanzhou (QZ), Hangzhou (HaZ), Kunming (KM), Chengdu (CD), and Beijing (BeJ) are selected as "checked cities" to independently evaluate the ability of the model's simulation and inversion. All of the 82 selected cities are shown in Figure 2. $\text{PM}_{2.5}$ concentrations at the 82 major Chinese cities are taken as the observations every two hours in the present study.

3. Numerical Experiments

Results obtained in previous studies indicated that the SSI produced high efficiency to interpolate a smooth and exactly fitting surface based on either scattered data or rectangular-grid data. According to Guo et al. [18], the inverted nonlinear

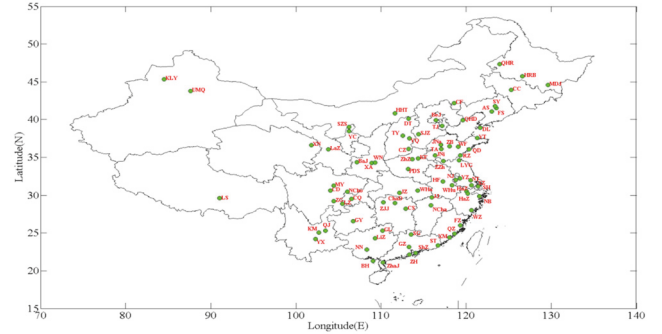


FIGURE 2: Map of computing area and the observation locations of 82 cities. The green dots denote the 82 cities used in the experiments. Full names of these cities can be found in [23].

parameter distribution was smoother than the surface constructed by the traditionally used linear interpolation in a two-dimensional tidal adjoint model. To evaluate the performance of the SSI, totally 12 twin experiments (TEs) are carried out and classified in two groups for the comparison with the CI results in the $\text{PM}_{2.5}$ adjoint model

For each experiment, we run the forward model with a prescribed IC field. The model-generated $\text{PM}_{2.5}$ concentrations at grid points of the observing positions shown in Figure 2 are regarded as the "observations". Considering the influence of the noises of in situ observations, we add an estimated maximum error of 5% to the "observations". The forward model is launched with an initial guess of ICs to obtain the simulations. Thereafter, the adjoint model is driven by the discrepancy between simulations and "observations". With variables obtained from the forward and adjoint models, gradients with respect to ICs are calculated. ICs at the independent points can be optimized according to (14). The ICs at other grids are determined by interpolation of the values at the independent points. Repeat the procedure with ICs being optimized until certain criteria are met. The optimization algorithm used in this work is the steepest decent method. And the criterion is that the number of iteration steps is equal to 300 at which the cost function can reach the minimum without large fluctuation. The flowchart of the process is shown in Figure 3.

Performance of the SSI or CI in combination of the adjoint model is evaluated by the mean absolute gross error (MAGE) [26] calculated as follows:

$$\text{MAGE} = \frac{1}{N} \sum_{i=1}^N |M_i - O_i| \quad (22)$$

where N is the number of observations and M and O are the modeled and observed results, respectively.

3.1. Results and Discussions of Group One. In Group one, two IC fields are prescribed (see Figure 6): a paraboloid opening downward (TE1) and a folding line distribution (TE2). The TEs focus on evaluating feasibility of the SSI in inversion of the ICs.

TABLE 1: Error statistics of the TEs in Group one before and after assimilation.

Experiment	J_{300}/J_1^a	K1 ^a ($\mu\text{g}/\text{m}^3$)		K2 ^a ($\mu\text{g}/\text{m}^3$)		K3 ^a ($\mu\text{g}/\text{m}^3$)		K4 ^a	
		Before	After	Before	After	Before	After	Before	After
SSI (TE1)	9.50e-4	32.81	0.97	29.03	0.89	6.33	1.14	13.34%	6.09%
CI (TE1)	1.96e-3	32.81	1.34	29.03	1.13	6.33	1.43	13.34%	6.66%
SSI (TE2)	1.73e-4	52.57	0.49	49.22	0.36	23.91	7.73	39.25%	14.64%
CI (TE2)	7.60e-4	52.57	1.04	49.22	1.12	23.91	7.87	39.25%	15.17%

^a J_{300} is the final value of cost function and J_1 is the initial value of cost function. K1 is the MAGEs between simulated values and “observations” in “assimilated cities”. K2 is the MAGEs between simulated values and “observations” in “checked cities. K3 and K4 are the MAGEs and MNGEs between prescribed and inverted IC, respectively.

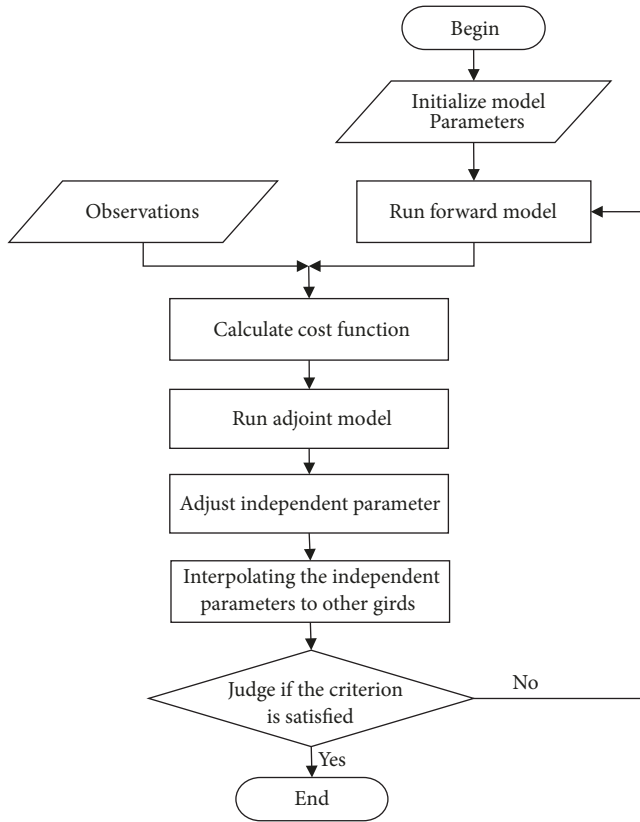


FIGURE 3: Flowchart of the experiments.

Figure 4 presents the iteration histories of the normalized cost function and MAGEs between the prescribed and inverted IC fields. As can be seen, the declining normalized cost function indicates that the misfit between the observations and model results is decreased and the observation data has been assimilated efficiently. Meanwhile, the decreased MAGEs suggest that the ICs are indeed optimized and getting close to the exact solution.

Results of the four TEs are summarized in Table 1. In TE1, it is apparent that the SSI shows an advantage over the CI in the model results. This is demonstrated by the normalized cost function values and the MAGEs between simulated values and “observations” in “assimilated cities” and “checked cities”. In addition, the SSI enables the MAGEs between the prescribed and inverted IC reduced by 81.99%, which is 4.58% better than the results obtained from the CI.

To further quantify the discrepancy between the prescribed and inverted ICs, the mean normalized gross error (MNGE) [26] is used and calculated as follows:

$$\text{MNGE} = \frac{1}{N} \sum_{i=1}^N \left[\frac{|M_i - O_i|}{O_i} \right] \quad (23)$$

The calculated results are listed in Figure 5. The MNGEs between the prescribed and inverted paraboloid opening downward at the initial iteration step are 13.34%, which are introduced by the difference between the initial guess values and the true values of the adjusted model ICs. After the assimilation, the CI gets the MNGEs reduced to 6.66%, while the SSI gets the MNGEs reduced to 6.09%.

In fact, it is a statement that the SSI provides better interpolation quality. Further evidence to support the conclusion can be seen through the inversion IC showed in Figure 6. As can be seen, the IC fields inverted by the adjoint model combined with both methods are consistent with the prescribed field. The SSI results display smoother pattern, confirming that the SSI shows superiority in reconstructing IC fields in the $\text{PM}_{2.5}$ adjoint model.

The same conclusions can be drawn from analysis of the TE2 results. The SSI results are superior to the CI results, manifested by the normalized cost function, MAGEs between simulated values and “observations”, and MAGEs between prescribed and inverted IC shown in Table 1. For the SSI simulations, the MAGEs between simulated values and “observations” in the “checked cities” before and after the assimilation are about two percent less than the CI simulations. The MNGEs between the prescribed and inverted folding line distribution at the initial iteration step are 39.25%. After the assimilation, the CI gets the MNGEs reduced to 15.17%, while the SSI gets the MNGEs reduced to 14.63%. Although the SSI gets the MAGEs and MNGEs between prescribed and inverted ICs slightly better than the CI, a smoother IC inversion also highlights the advantages of the SSI (Figure 6).

3.2. Results and Discussions of Group Two. The ill-posedness caused by incomplete number of the observation data is the key part needed to be solved in inversion problem. Feasibility of the SSI in inversion of the ICs is investigated by another group of twin experiments (Group two) under this assumption. According to the geographic distribution of the original 74 observation stations, the number of assimilated stations is

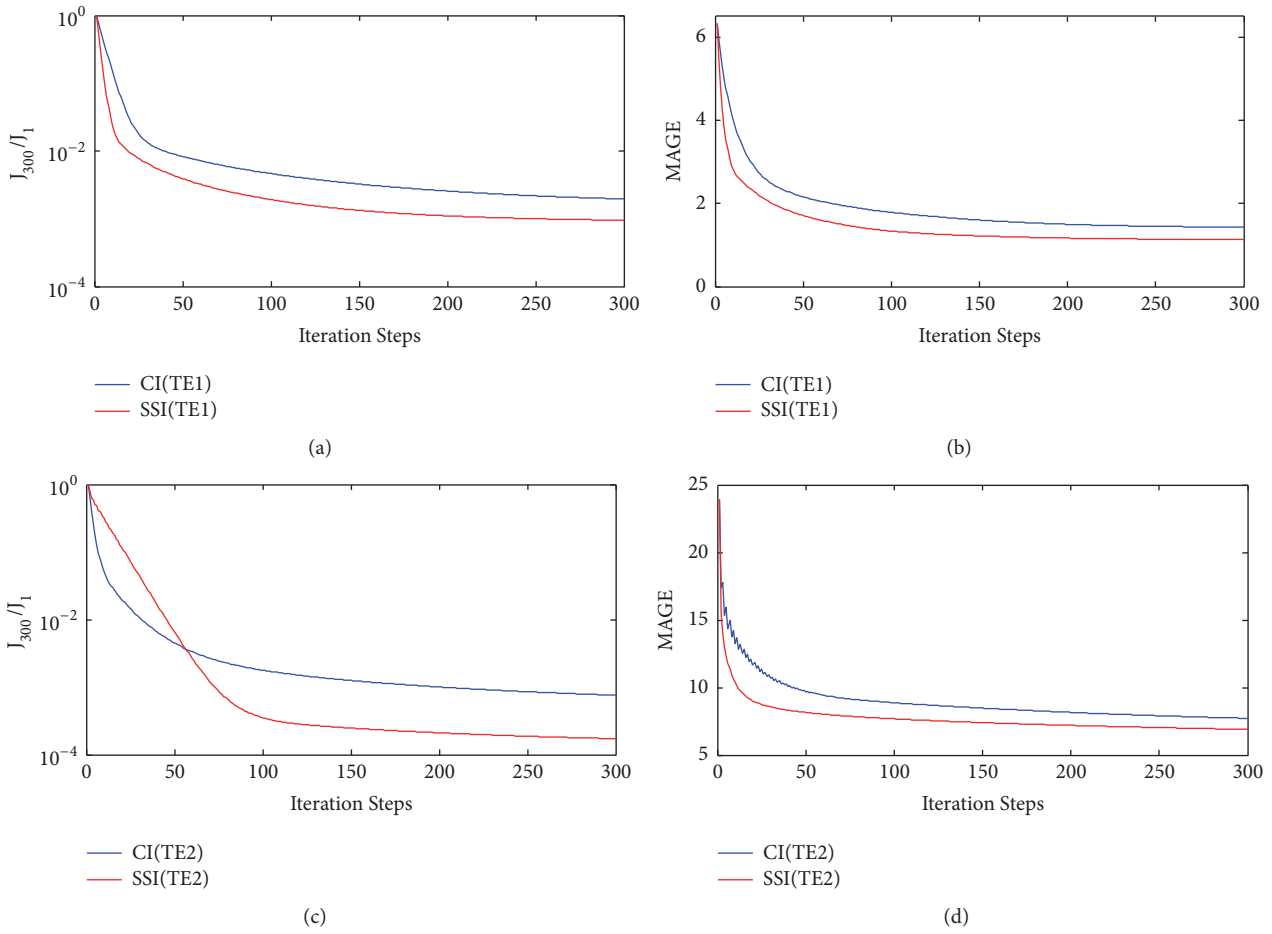


FIGURE 4: Iteration histories of the normalized cost function and the MAGEs between the prescribed and inverted ICs for Group 1.

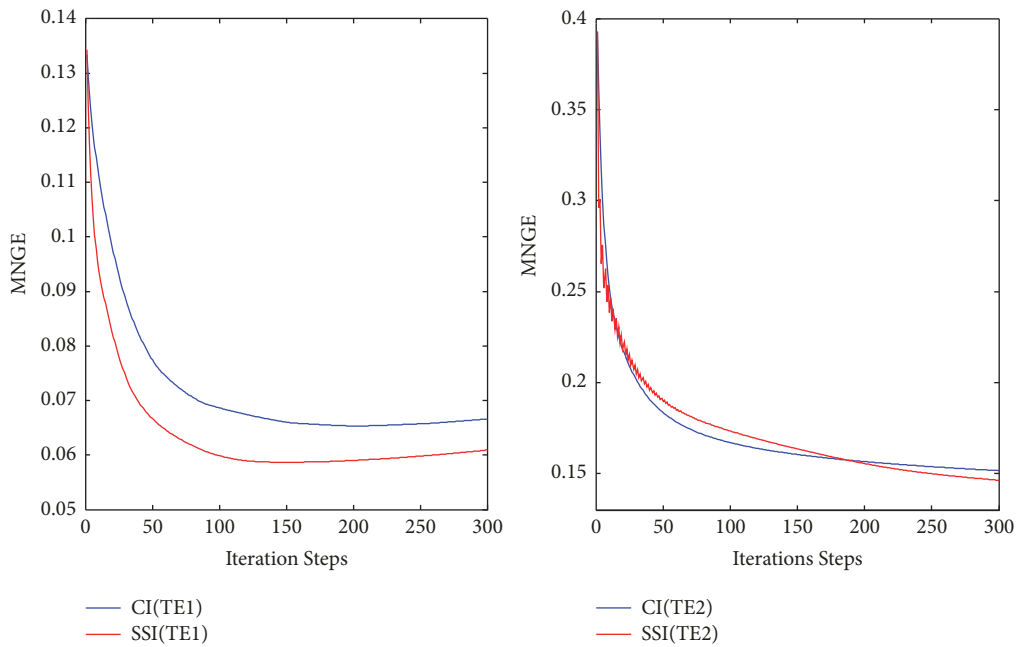


FIGURE 5: Iteration histories of the mean normalized gross errors (MNGEs) between the prescribed and inverted ICs for Group 1.

TABLE 2: Error statistics of TE3 and 4 and observations at 49 sites are assimilated in the TEs.

Experiment	J_{300}/J_1^a	K1 ^a ($\mu\text{g}/\text{m}^3$)		K2 ^a ($\mu\text{g}/\text{m}^3$)		K3 ^a ($\mu\text{g}/\text{m}^3$)		K4 ^a	
		Before	After	Before	After	Before	After	Before	After
SSI (TE3)	1.30e-3	30.49	1.06	29.01	0.98	6.33	1.18	13.34%	6.14%
CI (TE3)	2.75e-3	30.49	1.61	29.01	1.35	6.33	1.48	13.34%	6.74%
SSI (TE4)	9.56e-3	53.53	4.37	49.22	4.83	23.91	10.90	39.25%	23.48%
CI (TE4)	1.12e-2	53.53	4.88	49.22	5.35	23.91	11.21	39.25%	29.12%

^a J_{300} is the final value of cost function and J_1 is the initial value of cost function. K1 is the MAGEs between simulated values and “observations” in “assimilated cities”. K2 is the MAGEs between simulated values and “observations” in “checked cities. K3 and K4 are the MAGEs and MNGEs between prescribed and inverted IC, respectively.

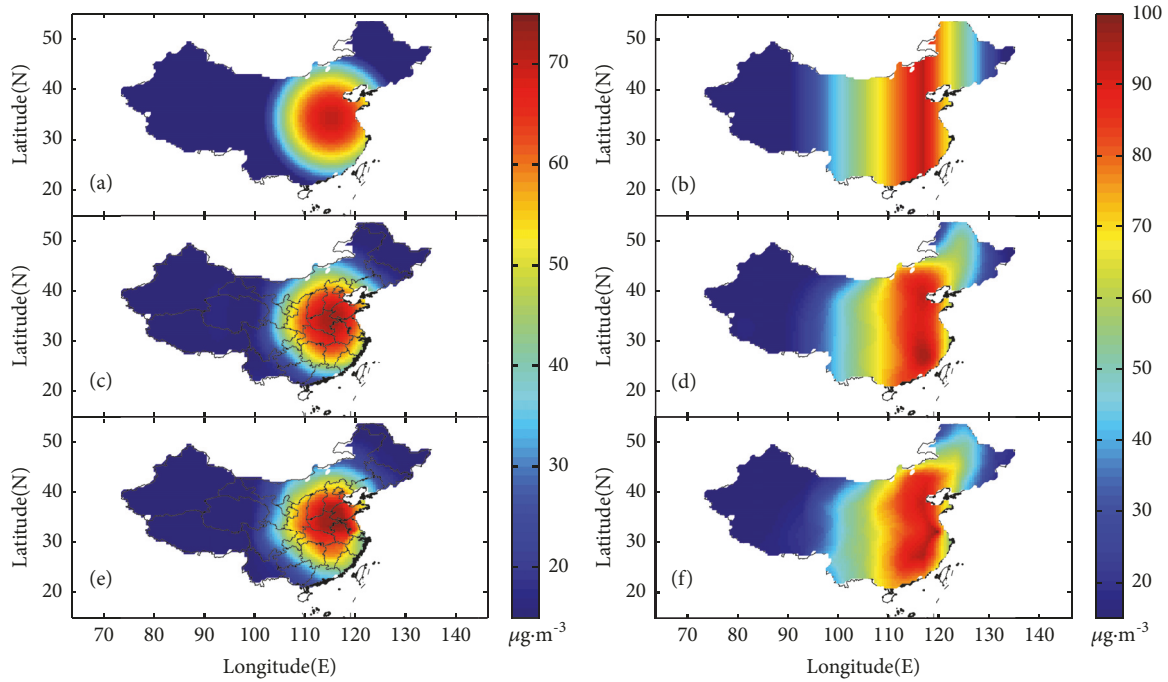


FIGURE 6: Two prescribed IC fields in twin experiments: (a) a paraboloid opening downward (TE1) and (b) a folding line distribution (TE2). The IC fields inverted combined with (c) the SSI and (e) the CI in TE1, (d) the SSI, and (f) the CI in TE2.

artificially reduced by a third and a half, respectively. The two kinds of prescribed IC fields in Group one are inverted in TE3 and TE4 by assimilating the observations at 49 observation sites. Meanwhile, data at 37 sites are taken as the observations in TE5 and TE6. Error statistics of the TEs in Group two are summarized in Tables 2 and 3. The assimilation procedures of the MAGEs and MNGEs between the prescribed and inverted ICs are shown in Figure 7.

As shown in Tables 2 and 3, the cost function can at least reach 10^{-2} of their initial value, indicating the successful ICs inversion in all the TEs. Our direct comparison of the error statics shown in Tables 1–3 indicates that the SSI results remain more accurate than the CI results in all the TEs of this group. Therefore, the following analyses are carried out based on the SSI results.

When the observations at 49 observation sites are assimilated in the adjoint model, the MAGEs between the prescribed and inverted folding line distribution in TE4 are at least 3.43% better than that obtained when 37 observation

sites are adopted in TE6. Meanwhile, the MNGEs in TE4 get a 0.64% advantage than that in TE6. Compared with the inversion of the folding line distribution, the inversion of the paraboloid opening downward is obviously affected by inadequate observations. The MAGEs between the prescribed and inverted paraboloid opening downward are 27.33% worse than that obtained when more observations are used. And the MNGE in TE3 is 1.48% worse than that in TE5. This is consistent with the conclusion obtained by Chertok and Lardner in [27] that the ICs inversions can be more efficient if the provided observations from sufficient number of sites can be used.

Further comparison of the ICs inversion errors demonstrate that the SSI results get less MAGEs and MNGEs than the CI results, when fewer observations are assimilated in the model. All the experiments indicate that the adjoint model combined with the SSI can much effectively overcome the ill-posedness caused by inadequate observations.

TABLE 3: Error statistics of TE5 and 6, observations at 37 sites are assimilated in the TEs.

Experiment	J_{300}/J_1^a	K1 ^a ($\mu\text{g}/\text{m}^3$)		K2 ^a ($\mu\text{g}/\text{m}^3$)		K3 ^a ($\mu\text{g}/\text{m}^3$)		K4 ^a	
		Before	After	Before	After	Before	After	Before	After
SSI (TE5)	1.32e-2	32.14	3.49	31.98	5.68	6.33	1.45	13.34%	7.62%
CI (TE5)	2.22e-2	32.14	4.56	31.98	6.02	6.33	1.48	13.34%	7.69%
SSI (TE6)	7.91e-3	52.64	4.04	49.36	5.97	23.91	11.77	39.25%	24.12%
CI (TE6)	9.81e-3	52.64	4.61	49.36	6.00	23.91	11.86	39.25%	25.95%

^a J_{300} is the final value of cost function and J_1 is the initial value of cost function. K1 is the MAGEs between simulated values and “observations” in “assimilated cities”. K2 is the MAGEs between simulated values and “observations” in “checked cities. K3 and K4 are the MAGEs and MNGEs between prescribed and inverted IC, respectively.

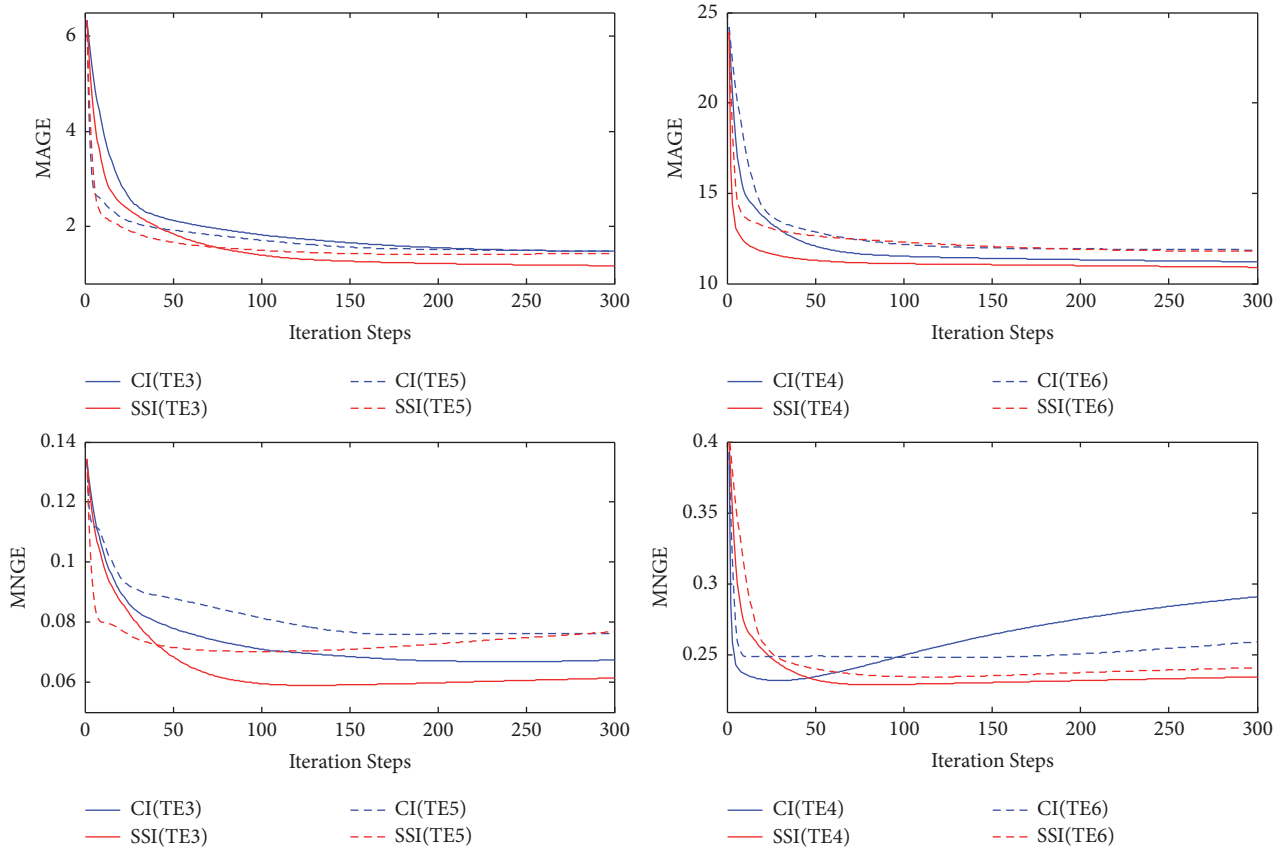


FIGURE 7: Iteration histories of the mean normalized gross errors (MNGEs) between the prescribed and inverted IC for Group 2.

4. Practical Experiments and Discussion

Performance of the adjoint model combined with the two methods is evaluated in a practical context. Hourly ground-level $\text{PM}_{2.5}$ observations (from 5 November to 11 November 2014) obtained from the Data Center of Ministry of Environmental Protection of the People’s Republic of China (<http://datacenter.mep.gov.cn/>) are assimilated into the model. These observations were measured based on the tapered element oscillating microbalance (TEOM) method (e.g., [10, 28]). Model-produced $\text{PM}_{2.5}$ concentrations are used for evaluation of the simulated results.

The inverted ICs are shown in Figure 9. On the whole, they show similar patterns that ICs including the northeastern, eastern, central, and northwestern regions are exposed to

hazardous levels of $\text{PM}_{2.5}$, which reflects the observations at 5 November 0:00 shown in Figure 8. However, according to the MAGEs between the observations and simulations in all the observation cities at the initial time shown in Table 4, the adjoint model with SSI gets a 2.06% advantage over that with CI. Meanwhile, with a closer inspection, it can be found that the IC surface obtained with SSI is much smoother while that with CI has bumps and depressions around several grids.

Statistical errors are shown in Table 4, which demonstrates that the $\text{PM}_{2.5}$ simulation is successful with both interpolation methods. The normalized cost function of the SSI and CI is 0.280 and 0.304, respectively. The SSI gets the MAGEs between simulated values and observations at the initial time to be 2.06% better than the CI results. Meanwhile, the MNGEs between simulated values and observations at the

TABLE 4: Error statistics of the practical experiment before and after assimilation.

Experiment	J_{300}/J_1^a	K1 ^a ($\mu\text{g}/\text{m}^3$)		K2 ^a ($\mu\text{g}/\text{m}^3$)		K3 ^a ($\mu\text{g}/\text{m}^3$)		K4 ^a	
		Before	After	Before	After	Before	After	Before	After
SSI	2.80e-1	37.87	20.82	42.93	22.15	40.23	24.27	48.88%	37.27%
CI	3.04e-1	37.87	21.65	42.93	23.40	40.23	25.10	48.88%	36.29%

^a J_{300} is the final value of cost function and J_1 is the initial value of cost function. K1 and K2 are the MAGEs between simulated values and observations in assimilated cities and checked cities, respectively. K3 and K4 are the MAGEs and MNGEs between the observations and simulated results in all the observation cities at the initial time.

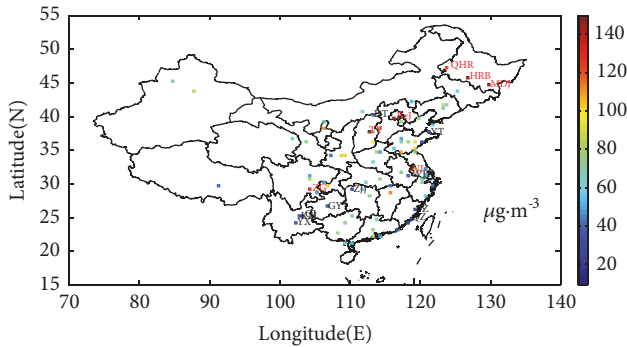


FIGURE 8: Observations at 5 November 0:00.

initial time have a 0.98% advantage, indicating superiority of the SSI. This statement is further validated by the MAGEs between observations and simulations in “assimilation cities” and “checked cities”. Simulations obtained with the SSI are used for further analysis of the model performance.

The values of mean simulations, normalized mean bias (NMB), normalized mean error (NME), and correlation coefficients are calculated as the statistical measures (e.g., [26, 28]) (domain wide averages) and plotted as an hourly time series in Figure 9. A closer inspection of the results indicates that the domain mean simulations show good agreement with the domain mean observations of the assimilation windows. As can be seen from Figure 10, the correlation coefficients, NMB, and NME values at initial time are 0.6289, -54.86%, and 55.36%, respectively, indicating the underestimations of $\text{PM}_{2.5}$. Since tapered element oscillating microbalance analyzers (TEOMs, which are commonly used in the EPA-China’s air quality monitoring network) measurements for $\text{PM}_{2.5}$ should be considered as lower limits because of volatilization of soluble organic carbon species in the drying stages of the measurement [26], the undersimulation is likely to be more severe than this evaluation suggests. This may be caused by the lack of the observations in the first few hours. In addition, the NMB ranges from -27.91% (2:00 Beijing time, 5 November) to 11.93% (16:00 Beijing time, 5 November), most of which is between -10% and 10%. The NME values are approximate to 25.18% which is the NME value of all the observations, indicating the stability of the adjoint model during the selected time. Meanwhile, the correlation coefficients between the domain mean simulations and mean observations are most between 0.80 and 0.95. These results show that the scheme can effectively assimilate the $\text{PM}_{2.5}$ observations.

The spatial distribution of simulated averaged $\text{PM}_{2.5}$ concentrations during assimilation window across China is shown in Figure 11. Coal combustion leads to seasonal high level of $\text{PM}_{2.5}$ concentrations in Northeast China in winter, which rose to 120-160 mg/m^3 during the assimilation window. Meanwhile, the concentrations are slightly large in middle and east coast of China, which is in conformity with industrial development. Mean $\text{PM}_{2.5}$ concentrations of Beijing are about 60 mg/m^3 , half values in the same period of previous years [29]. Air quality in Beijing and nearby provinces are better in the assimilation window, a period which coincided with the introduction of an emergency emissions-reduction strategy during the Asia-Pacific Economic Cooperation (APEC) summit in November. Above spatial distribution were consistent with findings from previous studies [30].

5. Summary

The independent point strategy serves as a satisfactory solution to overcome the ill-posedness of the inverse problem caused by excessive control variables. Spatially varying parameter is constructed by interpolating values at a group of independent points under this scenario. In this paper, the independent point strategy is described using the SSI as an alternative to the traditionally used linear interpolation. The adjoint model combined with the SSI is evaluated in simulation of $\text{PM}_{2.5}$ pollution in China by optimizing the ICs.

In twin experiments, the SSI results outperform the CI in the model simulations and inversion of nonlinear distribution of ICs. The IC fields reconstructed by the SSI are smoother than that by the CI. In addition, the SSI is verified to be more effective in solving the ill-posedness of the inversion problem than the CI. In practical experiments, ICs are optimized and the $\text{PM}_{2.5}$ concentrations in China are simulated by assimilating the ground-level observations during the 22th APEC. The comparatively accurate $\text{PM}_{2.5}$ distribution features demonstrate that the SSI plays a positive role in ICs inversion and simulations in practical application.

In conclusion, the SSI inversion strategy is feasible and better than the CI and can improve numerical results to some extent. We can obtain much smoother initial conditions which inverted with the SSI method and therefore are more in line with reality. And the improved IP scheme combined with the SSI is showing promise in the numerical model parameter inversions.

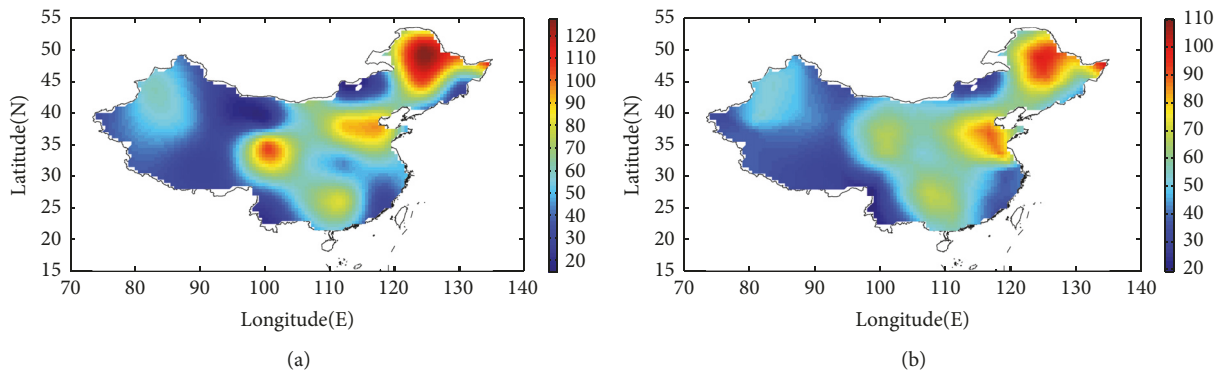


FIGURE 9: Inverted ICs obtained with the adjoint model combined with (a) SSI and (b) CI.

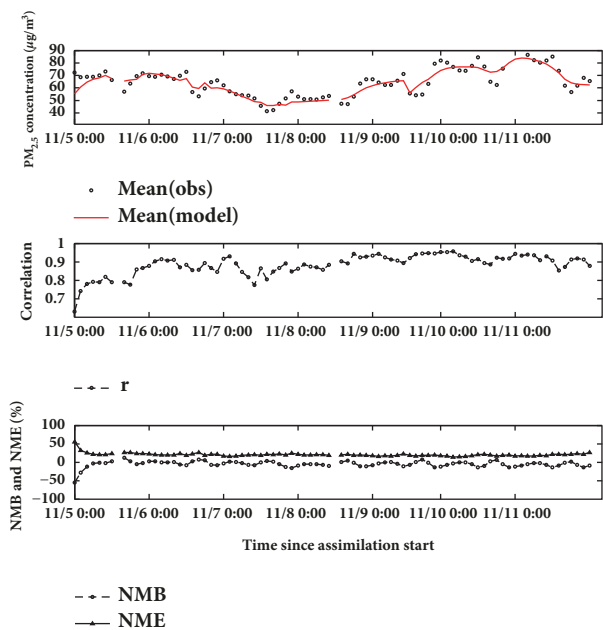


FIGURE 10: Comparison of the modeled and observed $PM_{2.5}$ concentrations based on the results from the SSI: temporal variation of domain mean, NMB, NME, and correlation.

Data Availability

All relevant data are available within the paper. The wind datasets are available from the NCEP Final Analysis (GFS-FNL) with spatial resolution of 2.5 degrees and temporal resolution every 24 hours. Hourly ground-level $PM_{2.5}$ observations are available from the Data Center of Ministry of Environmental Protection of the People’s Republic of China (<http://datacenter.mep.gov.cn/>).

Conflicts of Interest

The authors declare that there are no conflicts of interest regarding the publication of this paper.

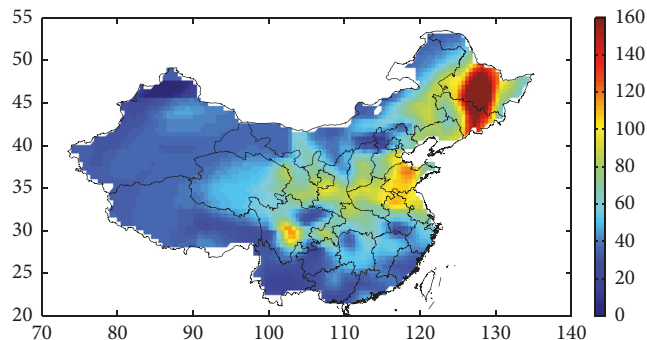


FIGURE 11: Spatial pattern of the average $PM_{2.5}$ concentrations ($\mu g/m^3$).

Acknowledgments

The authors highly appreciate the help and suggestions of the manuscript given by Daosheng Wang. And thanks are due to the surface spline numerical program provided by Haidong Pan. This work was partly supported by the National Key Research and Development Plan through Grants 2017YFC1404000 and 2017YFA0604100, the Natural Science Foundation of Zhejiang Province through Grant LY15D060001, and the Education Department Science Foundation of Liaoning Province of China (no. JDL2017019).

References

- [1] L. Han, W. Zhou, and W. Li, “City as a major source area of fine particulate ($PM_{2.5}$) in China,” *Environmental Pollution*, vol. 206, pp. 183–187, 2015.
- [2] Y.-R. Ma, Q. Ji, and Y. Fan, “Spatial linkage analysis of the impact of regional economic activities on $PM_{2.5}$ pollution in China,” *Journal of Cleaner Production*, vol. 2139, pp. 1157–1167, 2016.
- [3] H. Zhang, Z. Wang, and W. Zhang, “Exploring spatiotemporal patterns of $PM_{2.5}$ in China based on ground-level observations for 190 cities,” *Environmental Pollution*, vol. 216, pp. 559–567, 2016.
- [4] L. Han, W. Zhou, and W. Li, “City as a major source area of fine particulate ($PM_{2.5}$) in China,” *Environmental Pollution*, vol. 2139, pp. 1157–1167, 2016.

- [5] B. K. Pun and C. Seigneur, "Sensitivity of particulate matter nitrate formation to precursor emissions in the California San Joaquin Valley," *Environmental Science & Technology*, vol. 35, no. 14, pp. 2979–2987, 2001.
- [6] S. Yu, R. Mathur, K. Schere et al., "Evaluation of real-time $PM_{2.5}$ forecasts and process analysis for $PM_{2.5}$ formation over the eastern United States using the Eta-CMAQ forecast model during the 2004 ICARTT study," *Journal of Geophysical Research: Atmospheres*, vol. 113, no. 6, Article ID D06204, pp. 304–312, 2008.
- [7] C. Seigneur, "Current status of air quality models for particulate matter," *Journal of the Air & Waste Management Association*, vol. 51, no. 11, pp. 1508–1521, 2001.
- [8] D. K. Henze, J. H. Seinfeld, and D. T. Shindell, "Inverse modeling and mapping US air quality influences of inorganic $PM_{2.5}$ precursor emissions using the adjoint of GEOS-Chem," *Atmospheric Chemistry and Physics*, vol. 9, no. 16, pp. 5877–5903, 2009.
- [9] L. Zhang, L. Liu, and Y. Zhao, "Source attribution of $PM_{2.5}$ pollution over North China using the adjoint method," *AGU Fall Meeting Abstracts*, vol. 1, 2014.
- [10] S. Capps, D. K. Henze, and A. G. Russell, "Quantifying relative contributions of global emissions to $PM_{2.5}$ air quality attainment in the US," *AGU Fall Meeting Abstracts*, vol. 1, 2011.
- [11] S. C. Liu, S. A. McKeen, E.-Y. Hsie et al., "Model study of tropospheric trace species distributions during PEM-West A," *Journal of Geophysical Research: Atmospheres*, vol. 101, no. 1, pp. 2073–2085, 1996.
- [12] K. Fu and D. Liang, "The conservative characteristic FD methods for atmospheric aerosol transport problems," *Journal of Computational Physics*, vol. 305, pp. 494–520, 2016.
- [13] D. Wang, N. Li, Y. Shen, and X. Lv, "The parameters estimation for a $PM_{2.5}$ transport model with the Adjoint method," *Advances in Meteorology*, vol. 9, Article ID 9873815, pp. 1–13, 2016.
- [14] D. Wang, A. Cao, J. Zhang, D. Fan, Y. Liu, and Y. Zhang, "A three-dimensional cohesive sediment transport model with data assimilation: Model development, sensitivity analysis and parameter estimation," *Estuarine, Coastal and Shelf Science*, 2017.
- [15] D. Wang, J. Zhang, Y. P. Wang et al., "A methodology for estimating the parameters in three-dimensional cohesive sediment transport models by assimilating in situ observations with the adjoint method," *Journal of Atmospheric and Oceanic Technology*, vol. 34, no. 7, pp. 1469–1482, 2017.
- [16] D. Wang, J. Zhang, X. He et al., "Parameter estimation for a cohesive sediment transport model by assimilating satellite observations in the Hangzhou Bay: Temporal variations and spatial distributions," *Ocean Modelling*, vol. 121, pp. 34–48, 2018.
- [17] N. Li, Y. Liu, X. Lv, J. Zhang, and K. Fu, "The High Order Conservative Method for the Parameters Estimation in a $PM_{2.5}$ transport adjoint model," *Advances in Meteorology*, vol. 2017, pp. 1–13, 2017.
- [18] Z. Guo, H. Pan, W. Fan, and X. Lv, "Application of surface spline interpolation in inversion of bottom friction coefficients," *Journal of Atmospheric and Oceanic Technology*, vol. 34, no. 9, pp. 2021–2028, 2017.
- [19] G. D. Knott, "Interpolating cubic splines," *Progress in Computer Science and Applied*, vol. 11, pp. 319–321, 1999.
- [20] R. L. Harder and R. N. Desmarais, "Interpolation using surface splines," *Journal of Aircraft*, vol. 9, no. 2, pp. 189–191, 1972.
- [21] J. S. Wijnands, G. Qian, and Y. Kuleshov, "Spline-based modelling of near-surface wind speeds in tropical cyclones," *Applied Mathematical Modelling: Simulation and Computation for Engineering and Environmental Systems*, vol. 40, no. 19–20, pp. 8685–8707, 2016.
- [22] S. Yaghoobi, B. P. Moghaddam, and K. Ivaz, "An efficient cubic spline approximation for variable-order fractional differential equations with time delay," *Nonlinear Dynamics*, vol. 87, no. 2, pp. 815–826, 2017.
- [23] W. J. Qu, R. Arimoto, X. Y. Zhang et al., "Spatial distribution and interannual variation of surface PM_{10} concentrations over eighty-six Chinese cities," *Atmospheric Chemistry and Physics*, vol. 10, no. 12, pp. 5641–5662, 2010.
- [24] J. Zhang and Y. P. Wang, "A method for inversion of periodic open boundary conditions in two-dimensional tidal models," *Computer Methods Applied Mechanics and Engineering*, vol. 275, pp. 20–38, 2014.
- [25] D. Liu, J. Zhang, and S. Wang, "Constrained fitting of faulted bedding planes for three-dimensional geological modeling," *Advances in Engineering Software*, vol. 33, no. 11–12, pp. 817–824, 2003.
- [26] Y. Zhang, M. Bocquet, V. Mallet, C. Seigneur, and A. Baklanov, "Real-time air quality forecasting, part I: history, techniques, and current status," *Atmospheric Environment*, vol. 60, pp. 632–655, 2012.
- [27] D. L. Chertok and R. W. Lardner, "Variational data assimilation for a nonlinear hydraulic model," *Applied Mathematical Modelling*, vol. 20, no. 9, pp. 675–682, 1996.
- [28] Y. Zhang, M. Bocquet, V. Mallet, C. Seigneur, and A. Baklanov, "Real-time air quality forecasting, part II: state of the science, current research needs, and future prospects," *Atmospheric Environment*, vol. 60, pp. 656–676, 2012.
- [29] K. B. He, F. Yang, Y. Ma et al., "The characteristics of $PM_{2.5}$ in Beijing, China," *Atmospheric Environment*, vol. 35, no. 29, pp. 4959–4970, 2001.
- [30] J. L. Hu, Y. Wang, Q. Ying, and H. Zhang, "Spatial and temporal variability of $PM_{2.5}$ and PM_{10} over the North China Plain and the Yangtze River Delta, China," *Atmospheric Environment*, vol. 95, pp. 598–609, 2014.

